Statistics of defect trajectories in spatio-temporal chaos in inclined layer convection and the complex Ginzburg–Landau equation

Cristián Huepe and Hermann Riecke
Engineering Science and Applied Mathematics, Northwestern University, Evanston, Illinois 60208

Karen E. Daniels
Physics Department, Duke University, Durham, North Carolina 27708-0305

Eberhard Bodenschatz
Laboratory of Atomic and Solid State Physics, Cornell University, Ithaca, New York 14850
and Max-Planck-Institut für Strömungsforschung, Göttingen 37073, Germany

(Received 9 March 2004; accepted 14 June 2004; published online 16 September 2004)

For spatio-temporal chaos observed in numerical simulations of the complex Ginzburg–Landau equation (CGL) and in experiments on inclined-layer convection (ILC) we report numerical and experimental data on the statistics of defects and of defect loops. These loops consist of defect trajectories *in space–time* that are connected to each other through the pairwise annihilation or creation of the associated defects. While most such loops are small and contain only a few defects, the loop distribution functions decay only slowly with the quantities associated with the loop size, consistent with power-law behavior. For the CGL, two of the three power-law exponents are found to agree, within our computational precision, with those from previous investigations of a simple lattice model. In certain parameter regimes of the CGL and ILC, our results for the single-defect statistics show significant deviations from the previously reported findings that the defect dynamics are consistent with those of random walkers that are created with fixed probability and annihilated through random collisions. © *2004 American Institute of Physics.* [DOI: 10.1063/1.1778495]

Many nonequilibrium pattern-forming systems exhibit transitions from spatially ordered and temporally regular patterns to spatio-temporal chaos. Although much progress has been made, the identification and classification of different spatio-temporal chaotic states remains a challenge. The diagnostics for their spatial disorder and dynamics include, for example, correlation functions, power spectra, and attractor dimensions. To further clarify the nature of a given state of spatio-temporal chaos it is necessary to identify additional measures that reflect its specific aspects. In many systems topological defects appear to play a prominent role in disrupting the order of the pattern. In fact, it has been recognized that in certain two-dimensional equilibrium systems the (Kosterlitz–Thouless) phase transition from an ordered to a disordered state involves the unbinding of defects. In a model nonequilibrium system, a somewhat analogous defect-unbinding transition between an ordered and a disordered state of spatio-temporal chaos has recently been described. There, the transition was analyzed in terms of the statistics of defect trajectories and of loops that multiple trajectories form in space–time when connected via creation and annihilation events. In this paper we use this diagnostic tool to gain insight into defect-chaotic states obtained in simulations of the canonical complex Ginzburg–Landau equation and in experiments on inclined-layer convection (ILC).

I. INTRODUCTION

Various types of spatio-temporal chaos arise in a wide range of pattern-forming dynamical systems. While these systems have been investigated extensively in experiments and computations, a deeper understanding still poses interesting questions.

One of the central challenges concerns the origin of these states. In some cases the disordered states are not unexpected because all simple periodic states are linearly unstable. This is, for instance, the case in the complex Ginzburg–Landau equation [CGL, see (1) below] when the Benjamin–Feir instability[1] destabilizes all plane waves via spatial modulations that compress and expand them, or in rotating convection when the Küppers–Lortz instability renders all steady, spatially periodic roll states unstable to rolls of a different orientation.[2,3] In other situations, spatio-temporal chaos coexists with stable ordered states and finite-amplitude perturbations are needed to take the system from one attractor to the other. A striking example of this situation is spiral-defect chaos[4] in thermal convection in gases, which occurs despite the fact that straight-roll states are stable for the same values of the system parameters.[5] A similar situation occurs also in the CGL in certain Benjamin–Feir-stable regimes.[6] Recently, such bistability has also been identified in hexagonal patterns in the presence of rotation.[7,8] In a Swift–Hohenberg model for hexagonal patterns under the influence of rotation, penta-hepta defect chaos can be main-

tained by the ''induced nucleation'' of defects, in which penta-hepta defects trigger the nucleation of further defects, while regular hexagon patterns are actually linearly stable.[7] In rotating non-Boussinesq convection, numerical simulations have identified a regime in which a chaotic state is maintained through the interplay between defects in the hexagon pattern and whirling activity of the convection cells.[8] Similarly, bistability between undulation chaos and ordered undulations was found in inclined layer convection.[9]

Another challenge is to find characterizations of the disordered states that go beyond a description in terms of correlation functions. One interesting possibility to consider is a ''macroscopic'' description on large spatial and temporal scales. This approach has been successful in the case of the Kuramoto–Sivashinsky equation, which describes long-wave instabilities in various systems, including flame fronts,[10] falling fluid films.[11] This equation provides also the generic description of long-wave perturbations of spatially periodic traveling waves.[12] It has been shown[13–16] that on large length scales the spatio-temporally chaotic state obtained in the Kuramoto–Sivashinsky equation can be described by the noisy Burgers equation, which is also called the KPZ-equation.[17] While in the Kuramoto–Sivashinsky equation the diffusive term is destabilizing, the chaotic activity effectively renormalizes the diffusion coefficient to become positive, yielding the KPZ-equation with the noise term replacing the chaotic short-wave activity.

A large-scale description has also been obtained in a Ginzburg–Landau model for parametrically excited waves.[18–20] As is the case in many other systems, its steady periodic state can become unstable to spatial modulations of the pattern. In the limit of large wavelengths these perturbations can be described by a phase equation with negative diffusion coefficient.[21] Usually, the modulational instability leads to a change in the mean wave number of the system via phase slips. In this system, however, a regime has been identified in which the phase slips always occur in pairs. On larger time scales the wave number is therefore not changed, resulting in a chaotic state that has a well-defined wave number and in which the phase is conserved. As a result, in the long-wavelength limit perturbations of the chaotic state can be described by a new phase equation. Compared to the phase equation for the steady periodic state, its phase diffusion coefficient is renormalized by the chaotic activity. However, in contrast to the case of the Kuramoto–Sivashinsky equation discussed above the renormalized diffusion coefficient can itself change sign as a function of the mean wave number. This results in a chaotic state that is unstable with respect to long-wave modulations in its wave number and its chaotic activity. As a consequence, the system decomposes into domains in which double phase slips occur chaotically and domains with no phase slips in a process quite similar to phase separation in spinodal decomposition.

However, only very few states of spatio-temporal chaos allow a long-wave description. Since defects represent a conspicuous feature of many spatio-temporally chaotic states, it is tempting to use them to characterize the chaotic state and to obtain additional insight into its dynamics.[22] In one of the first attempts to do this, the probability distribution function (PDF) for the number of defects present at any given time was investigated in Ref. 23. For numerical simulations of the defect chaos in the CGL with periodic boundary conditions it was found that the PDF is well approximated by a squared Poisson distribution, which suggests a very simple picture for the dynamics of the defects. For a domain with periodic boundary conditions, a squared Poisson distribution is obtained if the defects behave as random walkers, created in pairs with a fixed probability and annihilated in random collisions with a defect of opposite charge. Distributions consistent with the squared Poisson distribution were subsequently also found in experiments on electroconvection in nematic liquid crystals[24] and in a reaction-diffusion model[25] simulated in a periodic domain.

In experiments on the anisotropic, defect-turbulent state of undulation chaos in ILC (see Fig. 9 below),[9] not only the distributions but also the defect nucleation and annihilation rates and, as necessary in any experimental system with a finite investigated area, the entering and leaving rates were measured. It was shown that the theoretical assumptions for the creation and annihilation rates[23] are justified for undulation chaos in a certain parameter regime and that a *modified* squared Poisson distribution function is found if entering and leaving rates are also considered. The fact that the nonperiodic boundary conditions lead to a modification of the distribution function indicates that the apparent agreement with the squared Poisson distribution found in the experiment on electroconvection in nematic liquid crystals[24] was fortuitous. In addition to measuring the rates, it was shown[9] that the dependence of the variance of the distribution on the mean number of defects was a better measure to distinguish the different PDFs. It was found that the modified Poisson distribution described this dependence well, while the squared Poisson distribution did not.

Defect statistics have also been investigated in recent simulations of the Willamowski–Rössler reaction-diffusion system with periodic boundary conditions.[26] In contrast to the situation in the complex Ginzburg–Landau equation, there the local dynamics are not periodic but chaotic.[27] Nevertheless, due to the structure of the chaotic attractor of the local dynamics, phase defects are well-defined and a squared Poisson distribution has been found.[26]

Strong deviations from the squared Poisson distribution were found in simulations with periodic boundary conditions of the spatio-temporal chaos in hexagons with rotation discussed above.[7] These deviations are due to the induced nucleation of dislocations by penta-hepta defects.

The dynamical relevance of defects has been addressed in three approaches. In simulations of the CGL (Ref. 28) it has been shown that the contribution of the defects to the Lyapunov dimension of the chaotic attractor can be extracted meaningfully, suggesting that each defect on average ''carries'' a certain amount of the Lyapunov dimension. It should be noted, however, that the background field behaves chaotically as well and therefore it contributes to the Lyapunov dimension even in the absence of defects. A related analysis was also performed in a reaction-diffusion model.[29] In another numerical experiment, based on spiral-defect chaos in Rayleigh–Bénard convection, it was shown that the system

is most sensitive to perturbations during the formation of dislocation pairs.[30] This suggests that defects may provide the origin of the chaotic dynamics. A third successful approach to describe a spatio-temporally chaotic state in terms of its defects has been presented recently.[31] There the velocity distribution function for the defect motion in the frozen vortex regime of the CGL has been captured quite well with simulations of point defects using their previously established interaction laws.

In this paper we employ a novel tool for the partial characterization of a spatio-temporally chaotic state that takes into account long-range aspects of the defect dynamics by investigating the statistics of the trajectories of the defects. To our knowledge, this tool has only been used before on a pair of coupled Ginzburg–Landau equations that model parametrically excited waves.[32,33] In a certain parameter regime, simulations of that system revealed a first-order transition between two chaotic states, one of which is spatially ordered and exhibits a spatially periodic correlation function while the other displays rapidly decaying correlations. The analysis of this transition was initially motivated by the assumption that for the spatial order of the state to be destroyed the defects in a pair would have to unbind, in a manner similar to the unbinding in the Kosterlitz–Thouless transition of the xy-model,[34] and the defects would thereafter have to separate over large distances. Investigation of the defect trajectories revealed, however, that this is not the case. It turned out that the entities to be considered are the loops formed in space–time by the trajectories of two or more defects that are connected to each other by being either created or annihilated together. In terms of these defect loops, the unbinding transition could be viewed as a transition from an exponential decay of the probability distribution function for the loop sizes to a power-law decay. Within the resolution of our statistics, the exponents of the power laws were found to agree with the exponents found in a simple lattice model in which the defects are replaced by random walkers.[33]

In the following, we first revisit the classic defect chaos state of the CGL. We find that for this state the form of the PDF for the number of defects depends on the parameters of the system and can deviate significantly from the squared Poisson distribution obtained previously, pointing to limitations of the mechanism assumed in Refs. 23–25. We then discuss the statistics of the defect loops, which for all parameter values investigated show power-law behavior. While two of the measured exponents agree well with those obtained in the disordered state of the parametrically excited waves,[33] one of them seems to depend on the parameters of the system. We then present results for the defect statistics obtained in experiments on undulation chaos in ILC (Ref. 9) and interpret them in view of the computational results.

II. DEFECT STATISTICS IN THE COMPLEX GINZBURG–LANDAU EQUATION

We investigate defect chaos in the two-dimensional complex Ginzburg–Landau equation (CGL)

$$\partial_t A = (1+ib_1)\Delta A + A - (b_3 - i)|A|^2 A \qquad (1)$$

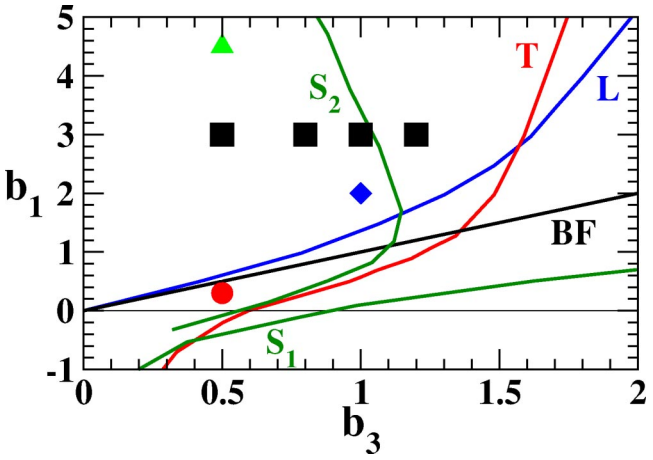

FIG. 1. (Color online) Phase diagram for the CGL following Ref. 6. Line BF denotes the Benjamin–Feir stability limit. Lines S_1 and S_2 denote the convective and absolute stability limit of the far-field of spiral defects, respectively. Defect chaos persists to the left of line T, while phase chaos exists between L and BF. The symbols denote parameter values for which defect statistics are presented here.

for the amplitude A of weakly nonlinear oscillations. The CGL exhibits various types of ordered and disordered states (for a review see Ref. 1). States of spatio-temporal chaos containing many defects, which in this system take on the form of spiral waves, arise over a wide range of parameters. Part of the phase diagram for the CGL is shown in Fig. 1.[6] In most of the parameter regime in which defect chaos persists (above line T), all spatially periodic plane waves are unstable with respect to long-wave modulations (above line BF denoting the Benjamin–Feir instability). The defect chaos also extends into regimes in which plane waves are still linearly stable over a range of wave numbers. There, the persistence of the chaotic dynamics is associated with the fact that the spiral defects emit waves with a wave number that is in the unstable regime.[35] More precisely, above line S_1 these waves are only convectively unstable, whereas to the left of S_2 they are absolutely unstable. As a result, random initial conditions lead to persistent defect chaos above and to the left of line T. In addition to defect chaos and the ordered plane waves the CGL exhibits a state of frozen defects (vortices)[36] to the right of line S_2 and phase chaos between the Benjamin–Feir line BF and line L.

As discussed in the Introduction, prior analysis of the defect-chaotic state investigated the probability distribution for the number of defect pairs in a periodic domain that are present in the system.[23] Within the accuracy of those simulations, the PDF was found to be consistent with a squared Poisson distribution over a range of parameters ($1.48 \leqslant b_3 \leqslant 1.11$ for $b_1 = 0.5$). This distribution arises if the defects are created with a fixed probability that is independent of their density, while they are annihilated according to a mass-action law. To test whether this description is valid even as the absolute stability limit is approached and crossed, we have measured the PDF in more extensive simulations with periodic boundary conditions. We use a pseudo-spectral code with integrating-factor Runge–Kutta time-stepping of fourth order. In these simulations we used $n = 128$ modes and a time

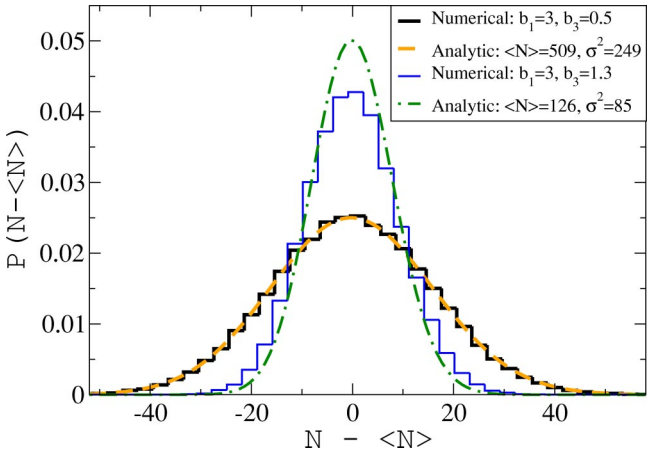

FIG. 2. (Color online) Probability distribution function for the number of defect pairs in the system. The analytic curves represent squared Poisson distributions for the values of $\langle N\rangle$ and σ^2 obtained from the corresponding numerical data.

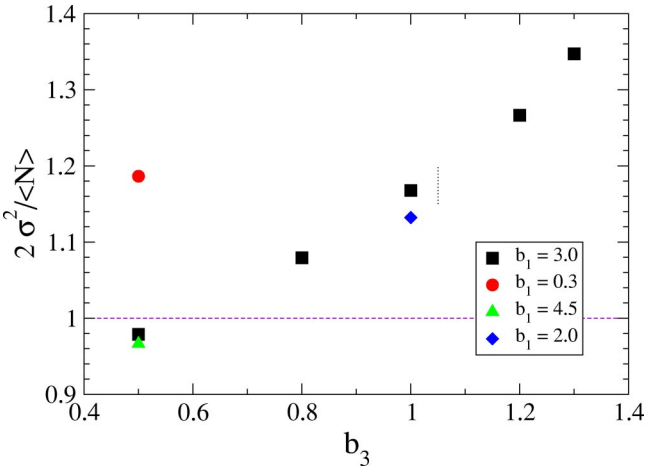

FIG. 3. (Color online) Dependence of the rescaled variance of the number of defect pairs, $2\sigma^2/\langle N\rangle$, on b_3 for various values of b_1. The absolute stability limit S_2 for $b_1=3$ is indicated by a dotted line. The dashed line corresponds to the squared Poisson distribution. The error in $2\sigma^2/\langle N\rangle$ is smaller than the symbol size.

step of $dt=0.25$. Halving the time step in selected simulations had almost no effect on the results while doubling the number of modes changed the mean number $\langle N\rangle$ of defect pairs by about 10% while the ratio $\sigma^2/\langle N\rangle$ of the variance to the mean was essentially unchanged (see below). The duration of these runs was $t_{\max}=10^6$.

Figure 2 gives the PDF for the number of defect pairs shifted by their mean in a system of size $L=308$. The parameters are $b_1=3$ with $b_3=0.5$ or $b_3=1.3$. For $b_3=0.5$, the PDF is well approximated by the squared Poisson distribution,

$$P(N)=\frac{1}{I_0(2\sqrt{\langle N^2\rangle})}\frac{\langle N^2\rangle^N}{(N!)^2}, \tag{2}$$

where I_0 is the modified Bessel function. As b_3 is increased above 0.8 the distribution becomes significantly wider. A quantitative measure of this change is the ratio $2\sigma^2/\langle N\rangle$ of the variance to the mean of the number of defect pairs, which satisfies $2\sigma^2/\langle N\rangle=1$ in the case of a squared Poisson distribution. The dependence of $2\sigma^2/\langle N\rangle$ on b_3 is shown in Fig. 3. The increased width of the PDF shows that the simple picture of random walkers with a fixed creation rate and pair annihilations in collisions is insufficient. We have not measured the creation and annihilation rates directly. At this point it is therefore not clear whether the deviations are mainly due to an increase of the creation rate with the defect density, as it has been found in the case of induced nucleation.[7] Alternatively, the increase of the annihilation rate could be slower than quadratic.

Our main objective is to investigate the defect trajectories and their statistics in the disordered regime. This is motivated by the fact that the equilibrium xy-model, which like the CGL is characterized by a single complex order parameter, undergoes a phase transition (Kosterlitz–Thouless) in which the system becomes disordered due to the unbinding of defect pairs.[34] To our knowledge, the dynamics of defects in the xy-model have not yet been studied in any detail. However, a first-order defect-unbinding transition has been found in a dynamical system modeling parametrically excited waves. There, the investigations of the defect dynamics showed that in the bound-defect regime the overwhelming majority of defect pairs appear only for brief periods of time.[32,33] Since the defects are annihilated by the same defects with which they were created, after the annihilation the pattern returns to essentially the same state as before the creation event and essentially no disorder is introduced. In contrast, jointly created defects that separate from each other modify the pattern in the domain between them: climbing defects change the wavelength of the pattern, while gliding defects induce a rotation of the pattern. Therefore, a seemingly natural and quite general expectation is that in order for defects to destroy the overall order of the pattern the defects in a pair have to move far from each other. For the specific system investigated in Ref. 32 it was shown, however, that even in the disordered regime this is not the case. Most defects are annihilated after a relatively short time and correspondingly travel only relatively small distances.

In Fig. 4(a) we present the cumulative probability distribution function (CPDF) for the average lifetime of individual defects in the CGL (1) over a range of parameters. Figure 4(b) gives the CPDF for the distance between the locations where a given defect was created and annihilated, respectively. Both quantities decay exponentially over the whole range of parameters investigated with a mean that is much smaller than the system size and than the duration of the simulation, respectively. Thus, the simple picture of defects separating far from each other does not apply to these disordered states.

The fact that the dynamics of individual defects only spans small spatial and temporal scales suggests that the relevant quantities for the destruction of order are not the single-defect statistics, but rather the statistical properties of the loops that are formed by the trajectories of many defects in space–time, connected through the annihilation and creation of defect pairs. An example of such a loop is sketched in Fig. 5, ignoring one space dimension (see also Fig. 13 below). To obtain the statistics of the defect loops we per-

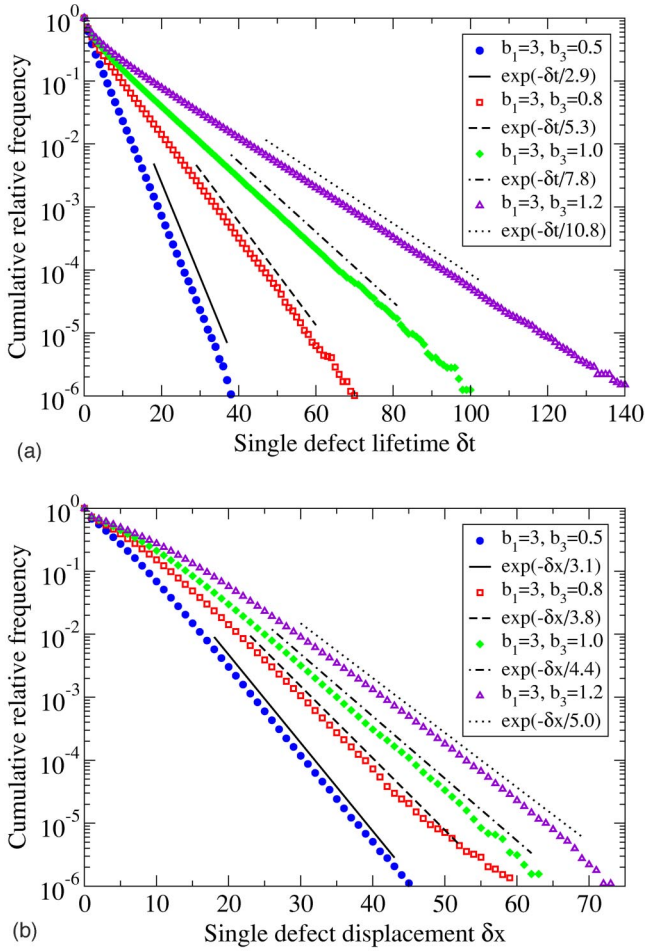

FIG. 4. (Color online) Cumulative probability distribution function for the defect lifetime (a) and for the distance between its creation and annihilation points (b).

formed simulations with $L=1232$, $n=512$, and $dt=0.25$ and tracked the defects as described previously.[33] The duration of the runs was either $t_{\max}=2500$ or $t_{\max}=5000$.

To obtain the defect trajectories we recursively check the distances between all defects $\mathcal{D}_i(t)$ at time t from all defects $\mathcal{D}_i(t+\Delta t)$ at time $t+\Delta t$. If for two defects of equal charge

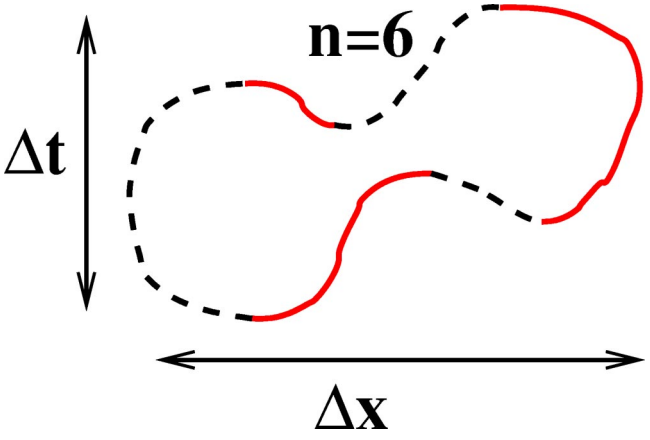

FIG. 5. (Color online) Sketch of a loop in space–time formed by the trajectories of six defects. Solid (dashed) lines indicate defects with positive (negative) topological charge.

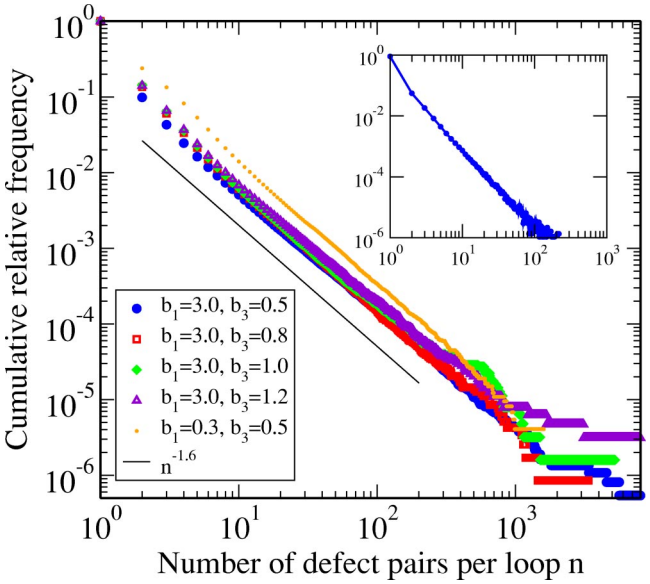

FIG. 6. (Color online) Cumulative probability distribution function for the number of defect pairs in a defect loop. System size $L=1232$ and duration of the simulations $t_{\max}=2500$ (except for $b_3=1.2$, for which $t_{\max}=5000$). Inset: Noncumulative distribution function for $b_1=3$ and $b_3=0.5$.

this distance is smaller than some threshold value $\delta_1^{(n)}=n\cdot\delta_1$ they qualify as a single "continuing defect" that has moved from one position to the other. It can happen that with this criterion a given defect $\mathcal{D}_k(t)$ has more than one possible continuation defect $\mathcal{D}_j(t+\Delta t)$. Then among the possible continuation defects the one closest to $\mathcal{D}_k(t)$ is assigned to be its continuation. Defects that are not "continuing defects" are candidates for annihilation and creation events. Among those, two defects of opposite charge and closer than a second threshold $\delta_2^{(n)}=n\cdot\delta_2$ are identified as a pair that was annihilated (or created) in this time step. This analysis is then repeated with increased values for the thresholds, $\delta_i^{(n+1)}=(n+1)\cdot\delta_i$, until all defects have been assigned.

Figure 6 shows the CPDFs for the number of defect pairs in a loop for the values of b_1 and b_3 marked by squares and by a circle in Figs. 1 and 3. Each point on these functions thus gives the probability of finding loops that contain at least the indicated number of defect pairs. The corresponding cumulative distribution function for the spatial extent of the loops is given in Fig. 7. Here the spatial extent is defined as the difference between the largest and the smallest x- (or y-) coordinate occurring in the loop (cf. Fig. 5). The cumulative distribution function for the similarly defined duration of the loops is given in Fig. 8. Note that even in this regime, in which the pattern is strongly disordered, most loops contain only a single defect pair, as shown in the inset of Fig. 6, which gives the noncumulative distribution function for $b_1=3$ and $b_3=0.5$. Thus, most defects are annihilated shortly after their creation by the same defect with which they were created. These events are unlikely to be responsible for the disorder in the pattern. All three distribution functions decay, however, with a power law,

$$C(n)\propto n^{-\alpha},\quad C(\Delta y)\propto \Delta y^{-\beta},\quad C(\Delta t)\propto \Delta t^{-\gamma}. \qquad (3)$$

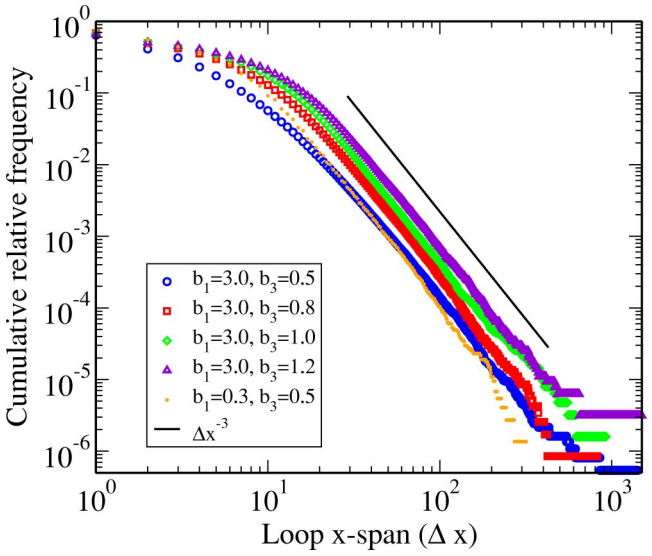

FIG. 7. (Color online) Cumulative probability distribution function for the maximal spatial extent Δx of a defect loop.

Thus, there is a non-negligible fraction of very large loops containing 1000 defects or more, extending over large parts of the system and persisting over substantial portions of the duration of the simulations. The power-law behavior is to be contrasted with the exponentially decaying distribution functions that were obtained previously for a spatially ordered, chaotic state.[33]

The exponents of the distribution functions for the number of defects and the spatial extent do not show a significant dependence on the parameters within the accuracy of our data and are given by $\alpha=1.6$ and $\beta=3.0$, respectively. Moreover, within the accuracy of the computations these exponents agree with the exponents found previously for a disordered state obtained in a model for parametrically excited waves[33] ($\alpha=1.5$, $\beta=3.0$) and a lattice model of random walkers that implements the assumptions underlying the squared Poisson distribution for the single-defect statistics[33] ($\alpha=1.6$, $\beta=2.9$). In Table I (see Sec. IV) these exponents are summarized, along with those obtained in the experiments discussed below.

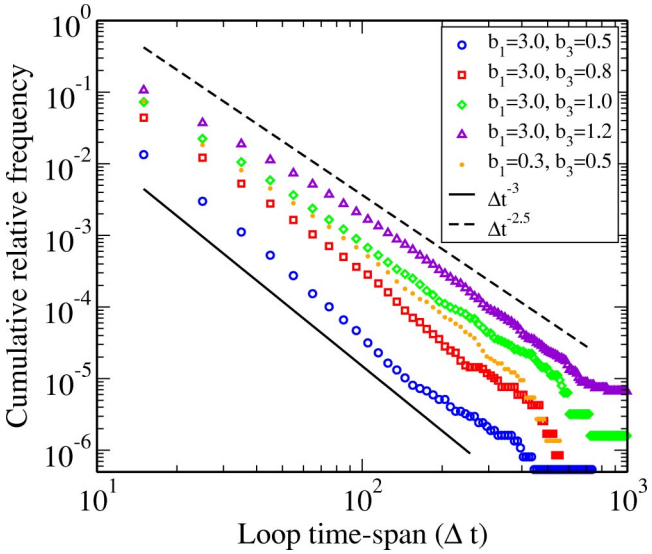

FIG. 8. (Color online) Cumulative probability distribution function for the maximal duration Δt of a defect loop.

By contrast, the exponent γ for the loop-duration CPDF may depend on the parameters. While far away from the absolute stability limit (line S_2) we obtain $\gamma\approx 3$, it appears that γ decreases to $\gamma\approx 2.5$ as S_2 is approached and crossed. At the present there is no theory that explains the existence of the power laws or gives values for their exponents and we can only speculate that the change in the exponent as line S_2 is approached may be related to our finding that in this regime the single-defect statistics deviate noticeably from the squared Poisson statistics. The quality of our data does, however, not rule out that the exponent γ is, in fact, independent of the parameters. In the previous analyses it was also found that the results for the loop-duration distribution function were less reliable than the others ($\gamma=2.7$ for the parametrically excited waves and $\gamma\approx 2.4$ for the lattice model).[33]

It should be noted that obtaining good statistics requires substantial amounts of data since the most relevant information is contained in the large loops. In a finite system with periodic boundary conditions the largest loops wrap around the whole system, which turns out to contribute to a slower decay of the distribution function for very large loops (cf. distribution function for $b_3=1.2$ in Fig. 8). Similarly, some loops persist for essentially the whole duration of the simulation. The cut-off by the finite duration of the simulations contributes, therefore, to a more rapid decay of the distribution functions for large loops (cf. distribution function for $b_3=0.8$ in Fig. 8). The statistics shown in Figs. 6, 7, and 8 are based on runs in which the mean number of defects at any given time is between 5000 and 15000 and in which of the order of 10000 snapshots are processed. Since our defect tracking scheme scales like the square of the number of defects in the system, a substantial increase in the system size investigated would require parallelizing the tracking scheme, which should be possible but would be a nontrivial task.

The power laws in the loop statistics reflect the sequential interaction of many defects and should therefore only be expected on scales that are larger than those associated with the individual defects. Indeed, the scales above which the distribution functions exhibit power-law behavior on Figs. 7 and 8 agree reasonably well with the mean distance traversed by the defects and their mean lifetime [cf. Figs. 4(a) and 4(b)].

III. UNDULATION CHAOS IN INCLINED-LAYER CONVECTION

In the following we present experimental results from undulation chaos (UC) in inclined layer convection (ILC) and compare them with the numerical results presented above. In ILC a thin fluid layer is heated from one side and cooled from the other. We define the angle of inclination Θ such that $\Theta=0°$ corresponds to the case of Rayleigh–Bénard convection,[37] where a horizontal fluid layer is heated from below and cooled from above. For any finite inclination angle, the component of gravity parallel to the fluid layer leads to a shear-flow with a cubic velocity profile, i.e., the

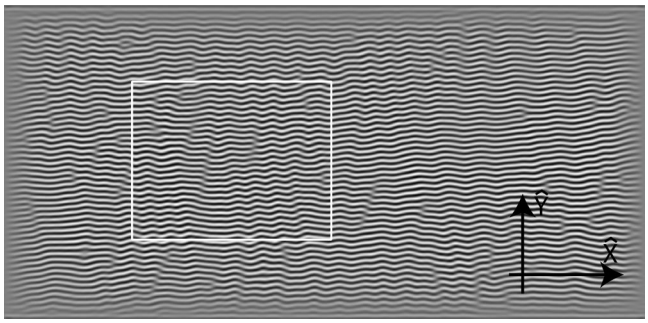

FIG. 9. Undulation chaos for $\epsilon = \Delta T/\Delta T_c - 1 = 0.08$ and inclination angle $\Theta = 30°$ as visualized with the shadowgraph technique. The whole convection cell is shown. In the subregion marked by a white box ($51d \times 63d$, where d is the height of the fluid layer) the spatio-temporally chaotic state was found to be homogeneous. All analyses shown in this paper were conducted for this subregion. Uphill is at the left side and the shearflow is along the $\hat{x}$-direction.

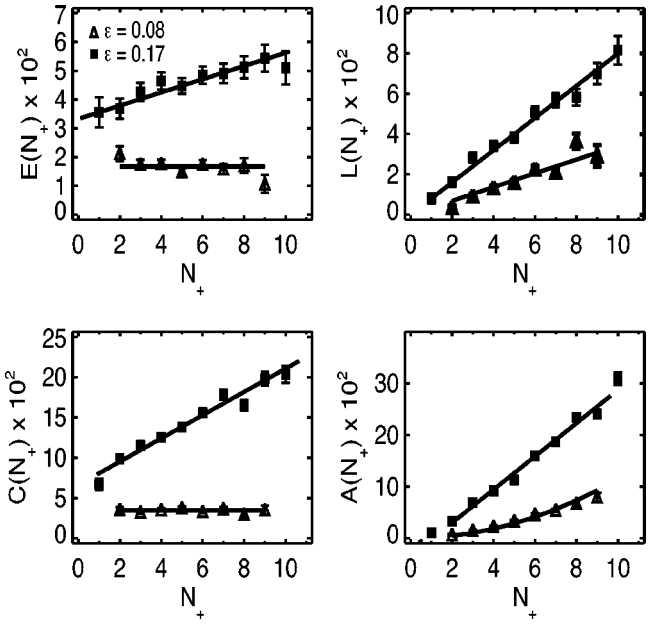

FIG. 10. Entering rate $E(N_+)$, leaving rate $L(N_+)$, creation rate $C(N_+)$, and annihilation rate $A(N_+)$ as a function of the number of positive defects in the cell for $\epsilon = 0.08$ (triangles) and $\epsilon = 0.17$ (squares). A similar dependence is found for negative defects.

fluid is rising along the warm side and falling along the cold side. Depending on the fluid parameters and for sufficiently small Θ, the primary instability above a critical temperature difference ΔT_c is to convection rolls whose axis is aligned with the shear-flow direction. These rolls have been termed longitudinal rolls in Ref. 38. In the case of compressed gases, where the thermal and viscous relaxation times are approximately the same, it has been shown that for intermediate angles longitudinal rolls are unstable to undulation chaos when the temperature is increased only slightly above critical.[9,39] A typical experimental picture of undulation chaos (UC) is shown in Fig. 9. The locations at which convection roll-pairs end or begin define topological defects. These defects are persistently created and annihilated, and move within the pattern. Here, we use the same experimental conditions as in Refs. 9, 40, 41 with $\Theta = 30°$, the cell height $d = (388 \pm 2)\ \mu$m and the viscous relaxation time $\tau_v = (1.532 \pm 0.015)$ s. As in the earlier work, we limit the investigation to a subregion of the convection cell where the behavior was found to be independent of the boundary conditions.[42] This subregion is marked by the white rectangle in Fig. 9. In addition, it needs to be noted that the whole convection pattern drifts slowly in the downslope direction (positive $\hat{x}$-direction), possibly due to non-Boussinesq effects. This can be observed in the movies that accompany the paper by Daniels and Bodenschatz.[9]

As reported earlier,[9] for intermediate angles two states of undulations were observed. For $0.01 < \epsilon < 0.1$ a defect-turbulent state of UC was found, characterized by the perpetual creation, annihilation, and motion of defects. Above $\epsilon = 0.1$, this state was found to compete with regions of ordered undulations without any defects, leading to intermittent dynamics.[9,42] It was observed that the mean number of defects increased to a peak near $\epsilon = 0.1$ and then weakly declined, with increased fluctuations above the transition to intermittency.[9]

In the region of pure UC ($0.01 < \epsilon < 0.1$), the creation and annihilation rates were measured as a function of defect density. The creation rates were found to be independent of defect density and the annihilation rates were found to be quadratic in the defect density (as shown in Fig. 10). As discussed before, these rates are consistent with the defects behaving like independent random walkers, leading to a squared Poisson distribution for the number of defects in a system with periodic boundary conditions. For any system with nonperiodic boundary conditions, however, which is typical for experimental systems, the fact that defects can enter and leave the observation window needs to be considered. The experimentally measured data for the entering and leaving rates as well as the creation and annihilation rates are shown in Fig. 10. As can be seen exemplarily for $\epsilon = 0.08$ the observed creation rate $C(N_+)$ was constant, the annihilation rate $A(N_+)$ was quadratic in the number of positive defects, the entering rate $E(N_+)$ was constant, and the leaving rate $L(N_+)$ increased linearly in N_+. With these rate relations, a modified squared Poisson distribution was derived.[9] A comparison of the different distributions is shown in Fig. 11(a), where the modified squared Poisson distribution fits the data for $\epsilon = 0.08$ best.

Above $\epsilon = 0.1$, this simple model breaks down, and, as can be seen exemplarily in Fig. 10 for $\epsilon = 0.17$, the observed creation rate increases with the number of defects and the annihilation rate does not follow a parabola. In other words, the defects interact strongly and the assumption of a short range interaction is no longer valid. Consequently, the modified Poisson distribution does not describe the PDF as shown in Fig. 11(b). Although this behavior is reminiscent of that found theoretically in penta-hepta defect chaos,[7] the underlying mechanism is not clear in the present case. Possibly, a coupling between the undulation and the roll pattern leads to the observed behavior.

As in the simulations, we tabulate single-defect statistics on the lifetime and displacement and find exponential distributions, as shown in Fig. 12. At $\epsilon = 0.17$ defects are observed to have shorter lifetimes and travel smaller distances than for

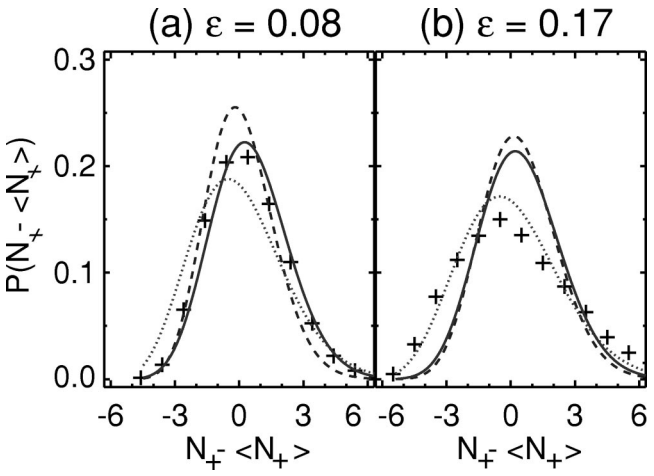

FIG. 11. Probability distribution functions for the number of positive defects in undulation chaos. The dotted line is the Poisson distribution, the dashed line the squared Poisson distribution, and the solid line the modified squared Poisson distribution. For $\epsilon=0.08$, $\langle N_+\rangle=4.6$ and for $\epsilon=0.17$, $\langle N_+\rangle=5.5$. A similar dependence is found for negative defects.

$\epsilon=0.08$. In addition, there are differences between the $\hat{x}$-displacement for defects with positive and negative topological charge especially for $\epsilon=0.08$. As described in Ref. 40, the velocity distributions of the defects are asymmetric with respect to the $\hat{x}$-direction. Positive defects move faster and more frequently in the upslope direction, while negative defects and the undulations do the opposite. As a result, there is a net drift of positive defects with respect to negative ones. Although we have no first-principle understanding of this behavior we attribute it to the non-Boussinesq effects that break the up–down symmetry.

Defect loop statistics in undulation chaos: In the study of loop statistics, we restrict our investigations to two experimental runs at ϵ typical for the two different regions. For $\epsilon=0.08$ ($\epsilon=0.17$) we tracked 5000 (15000) positive and negative defects for which both the creation and annihilation

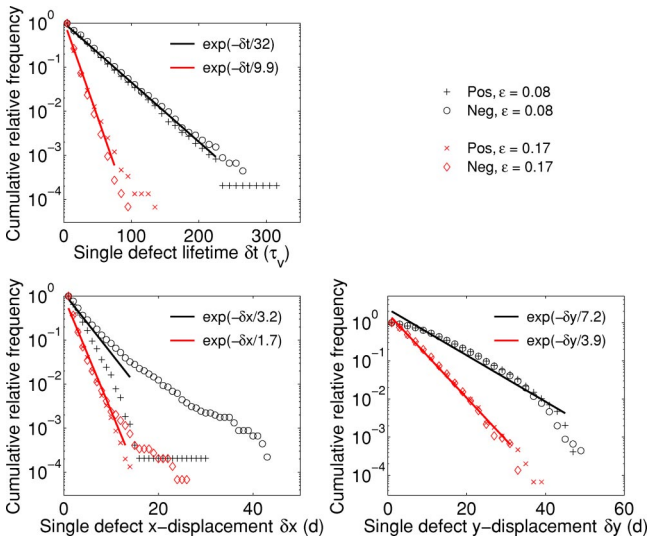

FIG. 12. (Color online) Cumulative single defect distributions for undulation chaos for $\epsilon=0.08$ and $\epsilon=0.17$. Fits to exponentials done over range shown.

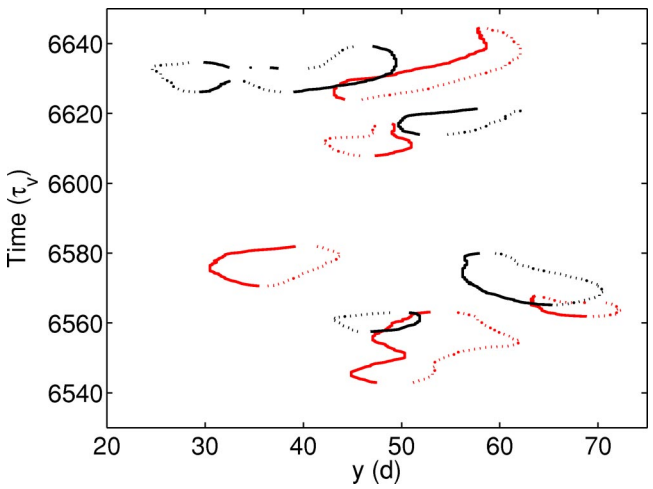

FIG. 13. (Color online) Space–time plot of defect loops in undulation chaos at $\epsilon=0.17$. Positive defects shown with solid lines, negative with dotted. A loop with $n=4$ pairs is shown in the upper left.

were observed. The data were taken over a time intervals of $1.7\times10^4\tau_v$ ($1.5\times10^4\tau_v$) with four (two) such runs at $\epsilon=0.08$ (0.17). We used previously developed techniques for defect tracking,[9] similar to those described above, to investigate the loop statistics analogous to the ones KD described in the theoretical investigations. Due to the finite observation area defects are gained and lost through the edges and not all observed defects participate in closed loops. The loss and gain of defects particularly affects the statistics of the large loops, since the statistics presented here use only those trajectories for which complete loops were available. For $\epsilon=0.08$ we analyzed 636 loops while for $\epsilon=0.17$ there were 3838 loops. An example of the measured loops is shown in Fig. 13. For clarity, this particular realization was chosen from an interval during which the defect density was low.

Figure 14 shows the cumulative distribution functions

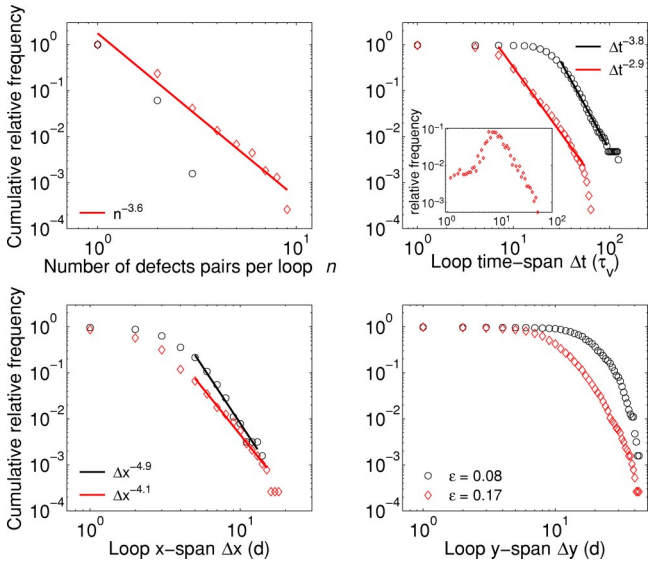

FIG. 14. (Color online) Cumulative loop distributions for undulation chaos at two values of ϵ. Fits to power law behavior done over range shown. The power exponents have an error of ±0.4. Inset in graph for Δt shows noncumulative relative frequency. Black circles are for $\epsilon=0.08$ and red diamonds for $\epsilon=0.17$.

corresponding to Figs. 6–8. As in the simulations, in spite of the fact that the state is disordered, we find that most loops consist of a single defect pair composed of two defects that mutually create and annihilate each other. While the system size and the amount of available data impose constraints on the results, we observe a sizable number of quite large loops and obtain cumulative distribution functions consistent with power laws for n, Δx (along the rolls) and Δt, particularly at $\epsilon = 0.17$. The onset of the power-law behavior in Δt occurs at about the lifetime of individual defects ($\delta t \approx 30\tau_v$ and $\delta t \approx 10\tau_v$ for $\epsilon = 0.08$ and $\epsilon = 0.17$, respectively). However, the onset of power laws for Δx occurs at larger distances than the single-defect behavior would predict. The exponents of the power laws are found to differ in the two regimes of UC, and the values of α and γ differ from those obtained in the numerical results presented above. A comparison of the values can be seen in Table I.

The experimental data show an additional feature not found in the simulations. As visible in the inset to Fig. 14, the noncumulative distributions for Δt, Δx, and Δy show a peak which is obscured in the cumulative plots. Such a feature indicates a characteristic size for the loops corresponding to $8\tau_v$, $10d$ ($\hat{y}$) and $2.5d$ ($\hat{x}$) at $\epsilon = 0.17$ and about twice these values at $\epsilon = 0.08$. The peak values are roughly in agreement with the decay constants associated with single-defect distributions (see Fig. 12).

Summarizing the experimental results, we have demonstrated that system-spanning defect loops are also present in an experimental system in spite of the difficulties presented by small system size and the flux of defects through the boundaries. The single-defect statistics were found to be exponential for the lifetime of the defects and the distance traveled. In agreement with the computational results, the loop statistics exhibit power-law scaling (for n, Δx, and Δt). The exponents at the two ϵ, however, do not agree well with each other. For example, for the time-span Δt in the intermittent regime of UC ($\epsilon = 0.17$) the exponent was 2.9 ± 0.4 and in the UC regime ($\epsilon = 0.08$) it was 3.8 ± 0.4. These should be compared with the numerical results of 2.5 to 3. While the two regimes may indeed be characterized by different exponents it is also possible that the difference in the measured exponents is due to the pronounced boundary effects and the limited data available. In particular, for $\epsilon = 0.08$ the number of observed loops was quite small and the convergence of the results may be in question. In addition, inclined layer convection is a highly anisotropic system with defect motion differing significantly in the two principle directions. In particular, in the $\hat{y}$-direction the defect motion often undergoes long flights[40] and the effect of the anisotropy on the loop statistics is unknown at this point. The fact that the loops have a characteristic size may also be relevant. Finally, the increased steepness of the power laws with respect to those found in the simulations may reflect the experimental bias against large loops due to the loss of defects through the edges.

Further experiments with a larger observation area and better statistics will be necessary to measure the exponents accurately enough to identify any system and parameter dependence. One prime candidate for an experimental investigation is electroconvection of liquid crystals where systems with large aspect-ratio can be built and spatiotemporal chaos exists close to onset.[24,43]

IV. CONCLUSION

In this paper we have applied a novel diagnostic measure for defect-dominated spatio-temporal chaos, the statistical properties of defect loops in space–time, to a canonical theoretical system (the complex Ginzburg–Landau equation) and to an experimental system (thermal convection in an inclined layer). In both cases we find that in the spatio-temporally chaotic state most loops are made up of only a single pair of defects that are created and annihilated together. Thus, in contrast to what might have been expected in a spatially disordered state, most defects do not separate far from each other after their creation. In fact, the probability distribution functions for the lifetime of individual defects and for the distance traveled during that time decay exponentially and yield mean values that are quite small. Therefore, we do not associate the origin of the disorder with a property at the single-defect level, but with the presence of large loops in space–time, which are formed by the trajectories of many individual defects connected via creation or annihilation events.

In both systems investigated, the probability distribution functions for the various quantities characterizing the loop sizes decay quite slowly, implying a significant number of large loops. In the simulations of the complex Ginzburg–Landau equation, the distribution functions follow power laws and loops containing more than 1000 defects and extending over large portions of the system occur relatively frequently. These large loops can be obtained since relatively large system sizes can be investigated. Moreover, due to the periodic boundary conditions used in the simulations, defects cannot leave the system. In the experiment, however, large loops are likely to include defects that are close to a boundary where the defects may leave the system without closing the loop. Such open loops have not been included in the statistics. Despite these finite-size effects, the experimental results also exhibit power-law behavior in some of the distribution functions. As in the simulations of the complex Ginzburg–Landau equation, the power-law behavior sets in at scales larger than those associated with the dynamics of the individual defects.

The numerical simulations of the complex Ginzburg–Landau equation yield exponents for the power laws that are consistent with those found previously for a model of parametrically excited waves and in a simple lattice model of random walkers.[33] In fact, two of the three exponents agree well with those obtained for those systems. A summary of the scaling exponents obtained in the various systems is shown in Table I.

So far, there exists no theory that would capture the power laws, let alone predict the values of the exponents. Thus, it is not known whether the exponents depend on features like the symmetries or the dimension of the system or the interaction between the defects. The agreement between the exponents obtained for the three computational systems

TABLE I. Summary of the exponents observed in a variety of defect-chaotic systems.

System	$\alpha\ (n)$	$\beta\ (\Delta x)$	$\gamma\ (\Delta t)$
Complex Ginzburg–Landau	1.6	3.0 ± 0.1	2.5 to 3.0
Parametrically excited waves[a]	1.6 ± 0.1	3.0 ± 0.2	2.8 ± 0.2
Lattice model[a]	1.6	2.9	2.4
Undulation chaos (UC), $\epsilon=0.08$	⋯	4.9 ± 0.4	3.8 ± 0.4
Intermittent UC, $\epsilon=0.17$	3.6	4.1	2.9

[a]Reference 33.

is therefore quite remarkable, since these systems differ substantially from each other. While the complex Ginzburg–Landau equation describes the weakly nonlinear behavior near a Hopf bifurcation, the parametrically excited waves arise effectively in a steady bifurcation, and the lattice model is a minimal stochastic model for diffusing defects. Moreover, the exponents for these systems agree also with those found in computations of a strongly anisotropic version of the complex Ginzburg–Landau equation,[44] in which the waves are Benjamin–Feir unstable only along one direction.[45] The exponents obtained in the experimental system differ noticeably from those found in the computations. At this point it is not clear whether this reflects a significant difference between the systems or is due to the more severe finite-size effects of the experiments. Numerical investigations of the biasing effects of truncated loops should be undertaken, along with further experiments on defect loops in large systems, as can be obtained in electroconvection of liquid crystals.

While we have focused here on situations in which the spatio-temporal chaos is dominated by defects, it should be noted that there are also spatio-temporally chaotic states without any defects. This is, for instance, the case in the phase chaos of the complex Ginzburg–Landau equation (e.g., Refs. 1, 6). In these systems the current approach is, of course, not applicable. Moreover, even in the defect-chaotic state of the complex Ginzburg–Landau equation the background phase field contributes to the Lyapunov dimension of the chaotic attractor on top of the contributions from the defects.[28] It may therefore be expected that in regimes like this the disorder is not only associated with the defect loops.

ACKNOWLEDGMENTS

H.R. and C.H. gratefully acknowledge support from the Department of Energy (DE-FG02-92ER14303) and from NASA (NAG3-2113). K.E.D. and E.B. thank the National Science Foundation for support through Grants Nos. DMR-9705410 and DMR-0305151. K.E.D. is also grateful for support from the NASA Microgravity Program (Grant No. NAG3-2372). E.B. and H.R. gratefully dedicate this paper to their Ph.D. advisor Lorenz Kramer in celebration of his 60th birthday, who infused them with his enthusiasm for physics, mountain climbing, white-water kayaking, and unicycling.

[1] I. S. Aranson and L. Kramer, "The world of the complex Ginzburg–Landau equation," Rev. Mod. Phys. **74**, 99 (2002).
[2] G. Küppers and D. Lortz, "Transition from laminar convection to thermal turbulence in a rotating fluid layer," J. Fluid Mech. **35**, 609 (1969).
[3] Y. Hu, W. Pesch, G. Ahlers, and R. E. Ecke, "Convection under rotation for Prandtl numbers near one: Küppers–Lortz instability," Phys. Rev. E **58**, 5821 (1998).
[4] S. W. Morris, E. Bodenschatz, D. S. Cannell, and G. Ahlers, "Spiral defect chaos in large aspect ratio Rayleigh–Bénard convection," Phys. Rev. Lett. **71**, 2026 (1993).
[5] R. V. Cakmur, D. A. Egolf, B. B. Plapp, and E. Bodenschatz, "Bistability and competition of spatiotemporal chaotic and fixed point attractors in Rayleigh–Bénard convection," Phys. Rev. Lett. **79**, 1853 (1997).
[6] H. Chaté and P. Manneville, "Phase diagram of the two-dimensional complex Ginzburg–Landau equation," Physica A **224**, 348 (1996).
[7] Y.-N. Young and H. Riecke, "Penta-hepta defect chaos in a model for rotating hexagonal convection," Phys. Rev. Lett. **90**, 134502 (2003).
[8] Y.-N. Young, H. Riecke, and W. Pesch, "Whirling hexagons and defect chaos in hexagonal non-Boussinesq convection," New J. Phys. **5**, 135 (2003).
[9] K. E. Daniels and E. Bodenschatz, "Defect turbulence in inclined layer convection," Phys. Rev. Lett. **88**, 034501 (2002).
[10] G. I. Sivashinsky, "Instabilities, pattern formation, and turbulence in flames," Annu. Rev. Fluid Mech. **15**, 179 (1983).
[11] G. I. Sivashinsky and D. M. Michelson, "On irregular wavy flow of a liquid film down a vertical plane," Prog. Theor. Phys. **63**, 2112 (1980).
[12] Y. Kuramoto, *Chemical Oscillations, Waves, and Turbulence*, Vol. 19 in Springer Series in Synergetics (Springer, Berlin, 1984).
[13] V. Yakhot, "Large-scale properties of unstable systems governed by the Kuramoto–Sivashinsky equation," Phys. Rev. A **24**, 642 (1981).
[14] S. Zaleski, "A stochastic model for the large scale dynamics of some fluctuating interfaces," Physica D **34**, 427 (1989).
[15] C. C. Chow and T. Hwa, "Defect-mediated stability: An effective hydrodynamic theory of spatiotemporal chaos," Physica D **84**, 494 (1995).
[16] M. Rost and J. Krug, "A particle model for the Kuramoto–Sivashinsky equation," Physica D **88**, 1 (1995).
[17] M. Kardar, G. Parisi, and Y. Zhang, "Dynamic scaling of growing interfaces," Phys. Rev. Lett. **56**, 889 (1986).
[18] G. D. Granzow and H. Riecke, "Phase diffusion in localized spatio-temporal amplitude chaos," Phys. Rev. Lett. **77**, 2451 (1996).
[19] G. D. Granzow, "Double phase slips and bound defect pairs in parametrically excited waves," Ph.D. thesis, Northwestern University, 1997.
[20] G. D. Granzow and H. Riecke, "Double phase slips and spatio-temporal chaos in a model for parametrically excited standing waves," SIAM (Soc. Ind. Appl. Math.) J. Appl. Math. **59**, 900 (1998).
[21] H. Riecke, "Stable wave-number kinks in parametrically excited standing waves," Europhys. Lett. **11**, 213 (1990).
[22] P. Coullet, L. Gil, and J. Lega, "Defect-mediated turbulence," Phys. Rev. Lett. **62**, 1619 (1989).
[23] L. Gil, J. Lega, and J. L. Meunier, "Statistical properties of defect-mediated turbulence," Phys. Rev. A **41**, 1138 (1990).
[24] I. Rehberg, S. Rasenat, and V. Steinberg, "Traveling waves and defect-initiated turbulence in electroconvecting nematics," Phys. Rev. Lett. **62**, 756 (1989).
[25] M. Hildebrand, M. Bär, and M. Eiswirth, "Statistics of topological defects and spatiotemporal chaos in a reaction-diffusion system," Phys. Rev. Lett. **75**, 1503 (1995).
[26] J. Davidsen and R. Kapral, "Defect-mediated turbulence in systems with local deterministic chaos," Phys. Rev. Lett. **91**, 058303 (2003).
[27] K. D. Willamowski and O. E. Rössler, "Irregular oscillations in a realistic abstract quadratic mass-action system," Z. Naturforsch. A **35**, 317 (1980).
[28] D. A. Egolf, "Dynamical dimension of defects in spatiotemporal chaos," Phys. Rev. Lett. **81**, 4120 (1998).
[29] M. C. Strain and H. S. Greenside, "Size-dependent transition to high-dimensional chaotic dynamics in a two-dimensional excitable medium," Phys. Rev. Lett. **80**, 2306 (1998).
[30] D. A. Egolf, I. V. Melnikov, W. Pesch, and R. E. Ecke, "Mechanisms of extensive spatiotemporal chaos in Rayleigh–Bénard convection," Nature (London) **404**, 733 (2000).
[31] C. Brito, I. S. Aranson, and H. Chaté, "Vortex glass and vortex liquid in oscillatory media," Phys. Rev. Lett. **90**, 068301 (2003).
[32] G. D. Granzow and H. Riecke, "Ordered and disordered defect chaos," Physica A **249**, 27 (1998).
[33] G. D. Granzow and H. Riecke, "Nonequilibrium defect-unbinding transition: Defect trajectories and loop statistics," Phys. Rev. Lett. **87**, 174502 (2001).
[34] J. M. Kosterlitz and D. J. Thouless, "Ordering, metastability, and phase

transitions in two-dimensional systems,'' J. Phys. C **6**, 1181 (1973).
[35] I. S. Aranson, L. Aranson, L. Kramer, and A. Weber, ''Stability limits of spirals and traveling waves in nonequilibrium media,'' Phys. Rev. A **46**, R2992 (1992).
[36] G. Huber, ''Vortex solids and vortex liquids in a complex Ginzburg–Landau system,'' in *Spatio-Temporal Patterns in Nonequilibrium Complex Systems*, edited by P. E. Cladis and P. Palffy-Muhoray (Addison-Wesley, Reading, 1995), pp. 51–62.
[37] E. Bodenschatz, W. Pesch, and G. Ahlers, ''Recent developments in Rayleigh–Bénard convection,'' Annu. Rev. Fluid Mech. **32**, 709 (2000).
[38] J. E. Hart, ''Stability of the flow in a differentially heated inclined box,'' J. Fluid Mech. **47**, 547 (1971).
[39] K. E. Daniels, B. B. Plapp, and E. Bodenschatz, ''Pattern formation in inclined layer convection,'' Phys. Rev. Lett. **84**, 5320 (2000).
[40] K. E. Daniels and E. Bodenschatz, ''Statistics of defect motion in spatio-temporal chaos in inclined layer convection,'' Chaos **13**, 55 (2003).
[41] K. E. Daniels, C. Beck, and E. Bodenschatz, ''Defect turbulence and generalized statistical mechanics,'' Physica D **193**, 208 (2004).
[42] K. E. Daniels, O. Brausch, W. Pesch, and E. Bodenschatz, ''Undulations and undulation chaos in inclined layer convection'' (in preparation).
[43] M. Dennin, G. Ahlers, and D. S. Cannell, ''Spatiotemporal chaos in electroconvection,'' Science **272**, 388 (1996).
[44] H. Riecke (unpublished).
[45] R. Faller and L. Kramer, ''Phase chaos in the anisotropic complex Ginzburg–Landau equation,'' Phys. Rev. E **57**, 6249 (1998).